Change Detection Algorithm for Multi-Temporal Remote Sensing Images Based on Adaptive Parameter Estimation

Chen, Yu; Ming, Zutao; Menenti, Massimo

DOI
10.1109/ACCESS.2020.2993910

Publication date
2020

Document Version
Final published version

Published in
IEEE Access

IEEE Access
Multidisciplinary | Rapid Review | Open Access Journal

Received April 18, 2020, accepted May 7, 2020, date of publication May 11, 2020, date of current version June 17, 2020.

Digital Object Identifier 10.1109/ACCESS.2020.2993910

Change Detection Algorithm for Multi-Temporal Remote Sensing Images Based on Adaptive Parameter Estimation

YU CHEN[1], ZUTAO MING[1], AND MASSIMO MENENTI[2]
[1]School of Geography and Information Engineering, China University of Geosciences, Wuhan 430078, China
[2]Department of Geoscience and Remote Sensing, Faculty of Civil Engineering and Geosciences, Delft University of Technology, 2628 CN Delft, The Netherlands
Corresponding author: Zutao Ming (cugmzt@139.com)

ABSTRACT This paper proposes a multi-temporal image change detection algorithm based on adaptive parameter estimation, which is used to solve the problems of severe interference of coherent speckle noise and the retention of detailed information about changing regions in synthetic aperture radar remote sensing images. The change area in the initial differential image has local consistency and global prominence. By detecting the significant area to locate similar change areas, the coherent speckle noise outside the area can be eliminated. The use of hierarchical FCM clustering to automatically generate training samples can improve the reliability of training samples. In addition, in order to increase the distinction between the changed area and the non-changed area, a sparse automatic encoder is used to extract the changed features and generate a change detection map. Experiments using 4 sets of SAR images show that the algorithm can effectively reduce the effect of speckle noise on detection accuracy, the extraction of changing areas is more complete and meticulous, and the false detection rate is greatly reduced. Since the images in different time phases will be disturbed by weather, clouds, sea water, etc., the target segmentation algorithm can be used to extract the target of interest and highlight the changing area. Principal component analysis and k-means clustering method are used to reduce the influence of isolated pixels, and change information is extracted to obtain different images. The experiment uses four sets of image data of islands and reefs. The experiment proves that the algorithm can well eliminate external interference, improve the accuracy of change detection, and have a good detection effect on the area of islands and reefs. The adaptive parameter estimation plays a good role in the detection of changing areas, and the visual effect is better, which can improve the accuracy of the detection results.

INDEX TERMS Adaptive parameters, multi-temporal, remote sensing images, change detection model, superficial superposition.

I. INTRODUCTION

With the development of remote sensing technology, the acquisition of high-resolution remote sensing data has become faster and the means are becoming more and more abundant. The era of high resolution has come and we are in the new century of remote sensing technology [1]–[5]. The high-resolution remote sensing image improves the spatial resolution of the image, shortens the change period of the remote sensing image, broadens the coverage, and enriches the image information. Real-time accurate change detection can help us better understand the features of the features and the progress of the natural environment, and manage and use the earth's resources. Change detection technology uses remote sensing images covering the same area to extract surface change information, which has been widely used [6]–[8]. High-resolution remote sensing image change detection technology has important applications in economic development, national defense construction, urban planning, environmental monitoring and other fields [9]. In agriculture, change detection technology can be applied to real-time monitoring of forest vegetation, agricultural crops, lake wetlands In economic construction, change detection technology can be used for urban planning management, illegal building

The associate editor coordinating the review of this manuscript and approving it for publication was Zhihan Lv.

extraction and monitoring and evaluation of natural disasters; militarily, change detection technology is used in military target detection, battlefield information dynamic perception, battlefield environment simulation plays an important role. Although high-resolution remote sensing images have high resolution and good imaging quality, due to the limitations of remote sensing imaging technology and the influence of noise interference, the extraction of changing areas still needs to be strengthened and improved, and it is necessary to develop and study changes with better applicability [10]–[15]. With the advancement of high-resolution remote sensing observation technology, the requirements for image quality have gradually increased [16]–[20]. High-resolution remote sensing images have become an important means of microwave remote sensing observation, which greatly enriches the content of change detection technology, have good application prospects in change detection and related fields, and has been extensively studied [21].

Gillespie AR and others proposed a fusion algorithm based on color normalization transformation (Brovey) [22]. The premise of using this algorithm is that panchromatic images and multi-spectral images have the same spectral response range, but there are some deficiencies in maintaining the spectral characteristics of the images. Jackson JE proposed the fusion algorithm of principal component analysis transformation (PCA) in the paper ''Principal Component Analysis User Guide'' [23]. The algorithm has no band limitation and the spectrum remains good, but the information is mainly concentrated in the first few principal components, he will change. Zhang *et al.* used the HSV color space model for image fusion in the paper ''Image Enhancement Using Mode-Selective Color Image Fusion'' and achieved the purpose of image enhancement [24]. Pathan *et al.* proposed an image fusion algorithm based on the Gram-Schmidt (GS) [25]. The GS transformation is not limited by the number of bands and can better save image information, but its anti-interference ability is not great, it takes a long time. The Rochester Institute of Technology (RIT) has proposed the Nearest Neighbor Diffusion Pan Sharpening (NNDiffuse) [26]–[30]. The advantage of this algorithm is that it better maintains the spectral information of the image and maintains the color [31]–[34]. High performance, Thyagharajan and Vignesh proposed an image fusion algorithm based on dual-tree complex wavelet transforms [35]. After this, Ji *et al.* proposed an image fusion algorithm based on current transformation [36].

In the threshold segmentation method, the pixels of the difference map can be divided into a change class and a non-change class by setting a threshold. Commonly used methods are the maximum between-class variance algorithm, Kittler algorithm and change vector analysis method [37]. Wickramasinghe *et al.* proposed an unsupervised model based on Bayesian theory and applied the expectation maximization algorithm to search for the optimal threshold [38]. Li *et al.* assumed that the distribution of changing and non-changing classes was Gaussian distribution, and proposed Kittler-Illingworth threshold selection criteria [39]. Marinelli *et al.* assumed that the distribution of changing and non-changing classes was non-Gaussian distribution, and used the generalized Kittler-Illingworth minimum error threshold algorithm to detect changes in SAR images [40]. The threshold method can produce a good classification effect when changed and non-changed classes of the statistical distribution belong to different modes in the histogram of the difference map. If the changing class and the invariant class cannot be accurately modeled by Gaussian or non-Gaussian distribution, the threshold model will not always produce excellent results, and this method is greatly affected by noise and the detection accuracy is not high [41]. Zhuang *et al.* proposed a threshold algorithm based on logarithmic mean for the detection of synthetic aperture radar image changes [42]. The difference image was generated by obtaining the logarithmic ratio of two SAR images, and the average value of the logarithm of each image was calculated [43]. The weight is multiplied by the minimum mean to obtain a weighted threshold to generate a different map. The algorithm has a short running time and a simple algorithm, and performs better in detection rate and Kappa coefficient [44]. Among the clustering methods, common methods include means clustering and fuzzy C-means (FCM) clustering. Hakkenberg uses the principal component analysis method to extract change features, and use the means method to cluster pixels into two categories to obtain a different map [45].

The development of remote sensing image change detection is getting better and better, and has made good progress in agriculture, military, scientific research. At present, there have been many advanced research results [46]. However, change detection of remote sensing started late, and the change detection technology and theory are far behind the remote sensing data acquisition technology. The detection technology is not mature and is still in the development stage. At present, there are still many difficulties in the detection of remote sensing image changes, and there are many problems that need to be solved, such as the lack of theoretical support. At present, most change detection methods lack the support of a theoretical foundation and mathematical models. In the process of algorithm implementation, empirical guidance is often used, such as selecting data sources, image preprocessing, selecting change detection methods, and evaluating the accuracy of results. High requirements for data preprocessing. Because the field of remote sensing image change detection is greatly affected by image quality, noise, whether seasonal changes, cloud cover, and shooting angle. The image preprocessing operations such as radiation correction, geometric correction, and image fusion are very strict, and the requirements for data quality are high. How to further remove interference and improve the accuracy of change detection is an important research topic. This paper summarizes the background significance and related theories of remote sensing image change detection, studies commonly used change detection algorithms, and analyzes the research status and existing problems with the algorithm. On this basis,

we mainly study the problem of detecting changes in SAR remote sensing images and high-resolution islands and reefs images, put forward corresponding solutions according to their respective characteristics, and verify the effectiveness of the algorithm through experiments.

(1) The SLIC superficial segmentation algorithm is integrated into the collaborative segmentation change detection algorithm. As the first step of the algorithm, multi-temporal images are super sensitized separately. In addition, through multiple sets of experiments on two experimental areas with different spatial resolutions, the optimal values of two important parameters in superficial segmentation were determined: compactness and segmentation step parameters.

(2) Using superposition analysis to achieve the unification of super-pixel segmentation of multi-temporal images, that is, after super-pixel segmentation of multi-temporal images, the multi-temporal images are superimposed, and different parts of the segmentation are extracted as new super-pixel superposition. In the original superficial segmentation, the unity of superficial objects obtained by segmentation in multi-temporal images is realized.

(3) A super-pixel-based collaborative segmentation change detection energy function is constructed. The energy function is divided into two parts: change feature and image feature. Both feature items are calculated using super pixels as the basic unit.

II. ADAPTIVE PARAMETER ESTIMATION TO ACHIEVE MULTI-TEMPORAL REMOTE SENSING IMAGE CHANGE DETECTION ALGORITHM

A. IMPROVED ALGORITHM IS BASED ON SPARSE ADAPTIVE PARAMETERS

In probability theory and statistics, probability distribution is a mathematical function that provides the probability of different possible outcomes of an experiment. In more specialized terminology, probability distribution describes the random phenomenon with the probability of an event. Probability distributions are generally divided into two categories [47]. Discrete probability distribution (applicable to situations where the set of possible outcomes is discrete, such as coin tossing or dice tossing) can be coded by a discrete list of probabilities of the results, called probability mass functions. On the other hand, a continuous probability distribution is usually described by a probability density function (a set of possible outcomes applicable to a scene can vary in a continuous range of values, such as the temperature of a certain day).

In calculating the relationship between the kernel function K (x) and the regularization operator P, it is possible to detect the generalization ability of certain kernel functions. This document also explains that the estimated distribution of the RBF kernel data is very smooth and often has good performance. The sparse representation can not only automatically construct the adjacency graph of sample points and avoid complicating parameter selection, but also, it can better reflect the geometric structure of the sample and obtain potential discriminant information. As a kind of structured sparse representation, group sparse has better sparse representation ability than general sparse representation. Inspired by improved Sparse Representation (MSR) proposed in [48], this paper proposes an improved group sparse framework (Modified Group Sparse, MGS). Different from the MSR framework, the MGS framework uses group sparseness to construct the adjacency matrix of samples, so as to obtain a higher level of sparseness of the sample matrix. In order to obtain the sparse coefficient matrix of the sample, the MGS framework solves the objective function shown in equation (1).

$$\min_{P} \sum_{i=1}^{n} \frac{1}{2} \left\| x_i - X_{P_i} \right\|_2^2 + \chi \left\| P \right\|_{2,1} \tag{1}$$

Sparse matrix P can reflect the similarity between sample points, and the similarity between similar samples is higher. According to the distribution characteristics of the samples, the samples of the same type are closer. That is, have higher locality. On the contrary, there is higher non-locality among heterogeneous samples. Therefore, using the sparse matrix P, the SUDP algorithm can directly describe the local and non-local relationships of the sample points. This process is implemented in the classic manifold learning algorithm using the K-NN algorithm. The use of K-NN algorithm inevitably requires the selection of k value, and the inappropriate k value often has a great influence on the algorithm. Using the sparse representation technique, the MGS framework can obtain the matrix S reflecting the local relationship of the sample points without determining the parameters, and the matrix S thus obtained naturally has discriminant information, which can improve the discriminant effect of the algorithm.

Use the obtained sparse matrix to describe the local information of the data set and construct the local sparse degree. Then the local sparseness can be expressed as equation (2).

$$Q_L(w) = \frac{1}{2} \sum_{i,j} (P_i - P_j)^2 P_{ij} \tag{2}$$

The optimization goal of local sparseness is to find the projection matrix w to minimize the distance between local points. For deriving equation (2) through a simple formula, equation (3) can be obtained.

$$\begin{aligned} Q_L(w) &= \frac{1}{2} \sum_{i,j} P_{ij} (w^T x_i - w^T x_j)^2 \\ &= \frac{1}{2} \sum_{i,j} P_{ij} (w^T x_i - w^T x_j)(w^T x_i - w^T x_j) \\ &= \frac{1}{2} w^T \Big(\sum_{i,j} P_{ij} (x_i - x_j)(x_i - x_j)^T \Big)^w \\ &= \frac{1}{2} w^T \Big(\sum_{i,j} P_{ij} (x_i x_i^T) + \sum_{i,j} P_{ij} (x_j x_j^T) - 2 \sum_{i,j} P_{ij} (x_i x_j^T) \Big)^w \\ &= \frac{1}{2} w^T (2XDX^T - 2\mathrm{XSX^T})^{\mathrm{w}} \\ &= w^T X (D - S) \mathrm{X^{Tw}} \end{aligned} \tag{3}$$

where D is a diagonal matrix, and each element of it is the row sum of the sparse matrix S. Let L = D-S, the local divergence can be expressed as:

$$Q_L(w) = w^T XLX^{\mathrm{Tw}} \tag{4}$$

After finding the local sparse matrix S, define the non-local sparse matrix SN is:

$$P_{ij}^N = 1 - P_{ij} \tag{5}$$

Correspondingly, the non-local divergence can be expressed as:

$$Q_N(w) = \frac{1}{2}\sum_{i,j}(1-P_{ij})^2(m_i - m_j) \tag{6}$$

After a simple formula transformation, each element in the diagonal matrix ND is assigned to the sum of the elements in each row of the matrix NS, and the non-local sparseness can be expressed as equation (7).

$$Q_N(w) = w^T XL_N X^{\mathrm{Tw}} \tag{7}$$

After describing the local and non-local information about the sample using local sparseness and non-local sparseness, the optimization goal of the SUDP algorithm is to maximize the non-local sparseness while minimizing the local sparseness. Therefore, the objective function of the algorithm is defined as equation (8).

$$Q(w) = \frac{Q_N(w)}{Q_L(w)} = \frac{tr(w^T XL_N X^{\mathrm{Tw}})}{tr(w^T XLX^{\mathrm{Tw}})} \tag{8}$$

The solution of equation (8) can be equivalent to solving the feature decomposition problem shown in equation (9).

$$tr(w^T XL_N X^{\mathrm{Tw}}) = tr(w^T XLX^{\mathrm{Tw}}) \tag{9}$$

The adaptive algorithm uses a sparse representation to construct the sample weight matrix, which is relatively time-consuming. Therefore, its time complexity will be higher than that of classic algorithms such as UDP. However, the sparse matrix obtained by sparse representation often has good discriminating ability, and the time-consuming process of selecting suitable parameter size by classic algorithms such as UDP is uncontrollable. From this point of view, it can be said that although the SUDP algorithm has a higher time complexity in theory than classic algorithms such as UDP, in practical applications, it's time performance may be better than the classic algorithm.

The non-local sparseness between classes is shown in equation (10).

$$Q_N(w) = \frac{1}{2}\sum_{i,j} P_{ij}(1-P_{ij})^2 + \left\|w^T X_b\right\|_2^2 \tag{10}$$

After formula transformation and matrixing, equation (10) is converted into equation (11).

$$Q_N(w) = w^T XL_N X^{\mathrm{Tw}} + w^T X_b X_b^T X^{\mathrm{Tw}} \tag{11}$$

After obtaining the intra-class sparseness and non-local sparseness, they are unified into a discriminant formula, as showed in equation (12).

$$Q_N(w) = \frac{Q_N(w)}{Q_L(w)} = \frac{tr(w^T XLX^{\mathrm{Tw}} + w^T X_l X_l^T X^{\mathrm{Tw}})}{tr(w^T XL_N X^{\mathrm{Tw}} + w^T X_b X_b^T X^{\mathrm{Tw}})} \tag{12}$$

B. CHANGE DETECTION MODELS OF MULTI-TEMPORAL REMOTE SENSING IMAGES

The detection model can set different layers of networks in the dense module, so that the model has a different network depths [49]. Let's take the 103-layer network in the detection model as an example. The network consists of an input layer, a 38-layer network with down sampling paths (including 4 Dense modules), a 15-layer Dense module, and a 38-layer network with up sampling paths (including 4 Dense module), consisting of a convolutional layer and Softmax layer, a total of 103 layers of network. The specific network settings are shown in Figure 1.

After pre-processing the original images, super-pixel segmentation can be performed on the original images of different times in the same area. The algorithm steps are described in detail before, so they will not be described here. Although the two-phase image after superficial segmentation has the same number of superficial, the segmentation boundaries of the two superpowers must not correspond to each other. Super pixel segmentation cannot rely solely on the segmentation boundary of one phase as a standard, so in order to facilitate the next collaborative segmentation, the superficial segmentation boundary needs to be unified. Therefore, this study superimposes the two-phase superficial segmentation boundaries, filters extracted patches as new superficial and overlays the original segmentation boundary, to obtain a unified comprehensive superficial segmentation boundary. The specific process is shown in Figure 2.

Super pixel superposition analysis needs to superimpose two superficial images to extract patches with different divisions between them. It can be seen from (c) that most of the extracted plaques are some long and unit area interference plaques. The analysis found that these interference plaques are mostly located at the boundary of superficial, mainly due to the two phases. The image is caused by a deviation of one of half a pixel. Therefore, in this study, two screening conditions were set to remove interfering plaques: remove the patches of unit area (1-2 pixels); remove the patches of area perimeter ratio <8.

The autoloader can obtain the features representing the input data. When extracting features, you can add constraints to the hidden layer so that it can obtain excellent sample features under poor conditions [50]. The sparsity limit can be used to constrain the hidden layer, which is more conducive to obtaining the main characteristics of the input data, and can effectively reduce the dimension of the sample and eliminate redundant information. Because the deep neural network based on Sparse Automatic Encoder (SAE) has a good learning feature function, this paper uses the sparse automatic

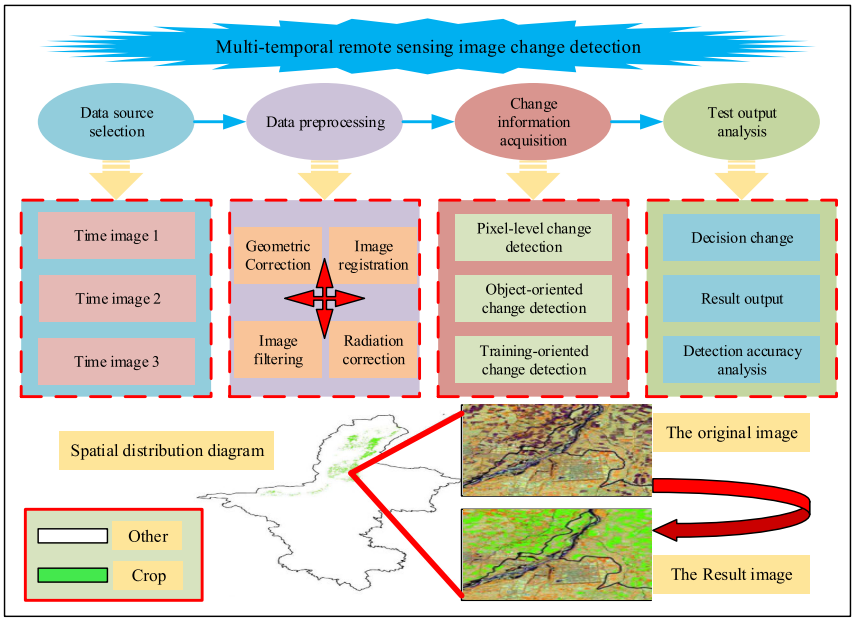

FIGURE 1. Framework of change detection model for multi-temporal remote sensing images.

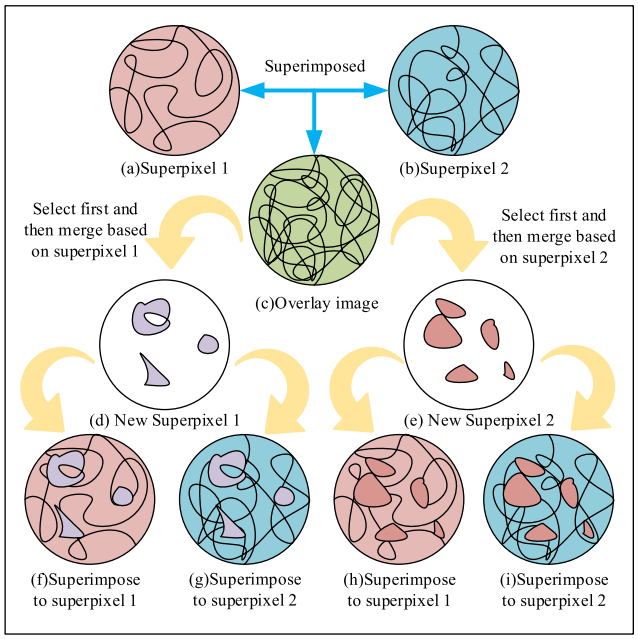

FIGURE 2. Flow chart of overlay analysis.

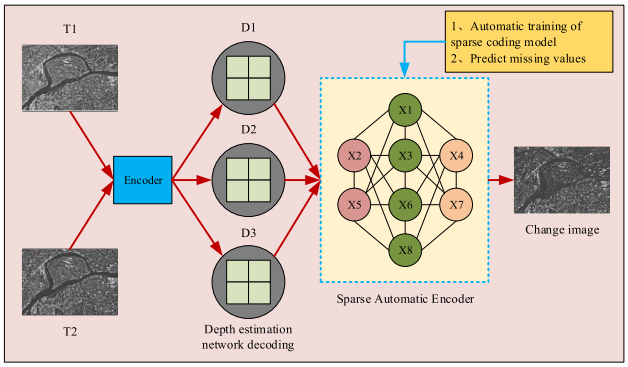

FIGURE 3. Flow chart of sparse automatic encoder change detection.

encoder to extract the change information of multi-temporal SAR remote sensing image and suppress the speckle noise.

In order to prevent useful information that may be lost during the generation of the difference map, the two original SAR images after the salient region detection process and the neighborhood pixel features of the difference map are input to SAE to learn more effective changing features, compared to using only the difference map The extraction effect is better. The resulting data are input into the sparse autoloader network for training. Each network layer is composed of a sparse autoloader. The hidden layer of each network is used as the input of the next layer of the network, and the network with two hidden layers is used. To extract the features of the input data. The output feature of the last hidden layer is used as the input of the surtax classifier, and the pixels are divided into variable and non-variable classes by the classifier to obtain the final change detection result. Figure 3 shows the flow chart of sparse automatic encoder change detection.

C. MULTI-TEMPORAL REMOTE SENSING IMAGE CHANGES DETECTION PARAMETERS AND EXPERIMENTAL DATA

The specific algorithm step parameters of the adaptive multi-temporal remote sensing image change detection are shown in Table 1.

After the construction of the energy function is completed, the image features and change features of each pixel are calculated, and then the two features of all pixels in the super pixel block are averaged to obtain the image features and

TABLE 1. Specific algorithm step parameters for the change detection of adaptive multi-temporal remote sensing images.

Step	Description
1	Use the PCA algorithm to reduce the entire data set to a certain dimension to solve the problem of small samples in the data set.
2	Divide the sample set X into c sample subsets according to the category label.
3	Use the supervised sparse framework to find the adjacency matrix S of the training set.
4	Use equation (1) to find the sparse reconstruction coefficient Si of each sample.
5	Arrange the sparse reconstruction coefficients corresponding to each sample into an adjacency matrix S.
6	Use the S matrix obtained in step 3 to construct a local Laplace matrix.
7	Use W to project the entire data set into a low-dimensional space, use the KNN classifier to determine the category of the unknown image.

TABLE 2. Mixture matrix.

Types		Forecast category	
		Outlier	Normol
Actual category	Outlier	Predict the correct Outlier (TN)	Outlier with wrong prediction (FP)
	Normal	Normal with wrong prediction (FN)	Predict the correct Normol (TP)

change features of the super pixel. Collaborative segmentation is to optimize the energy function and finally complete the image segmentation. The optimization of the energy function is achieved by obtaining the minimum cut of the network flow graph. The minimum cut / maximum flow algorithm is an energy function optimization method. First, the superficial image needs to be mapped to a network flow graph, and then the minimum cut of the network flow graph is obtained. The network flow graph is constructed as follows: take each superficial block as an ordinary node, and then set two special nodes S (target) and T (background), connect the nodes with edges, connect the two special nodes to each An ordinary node is connected, which is an edge sum, and an ordinary node is connected to its adjacent ordinary node (this article uses four neighbors), which is an edge. Then, the changed feature item is regarded as the weight of the edge between the two special nodes and the ordinary mode; the image feature item is regarded as the weight of the edge between the two ordinary nodes. At this point, the network flow graph is completed.

The confusion matrix is an evaluation method for the quality of outlier detection. If the data set contains class labels, the concept of the ledger can be used to evaluate the effectiveness of outlier detection methods, such as accuracy and recall, based on the class labels. Rates, false positive rates, and others, in the absence of class labels, can also be verified by removing the outlier data model. Obviously, as showed in Table 2, the confusion matrix mainly contains four parts of information.

Represents the ratio of correctly predicted points in normal data to the sum of predicted wrong data in erroneous data. Accuracy represents the accuracy of predictions in positive sample results. The higher the value, the better it is. The accuracy rate is defined as:

$$M = \frac{TM}{TM + FM} \tag{13}$$

There are four sets of experimental data used in this paper, which are SAR images of Bern, San Francisco, Red River,

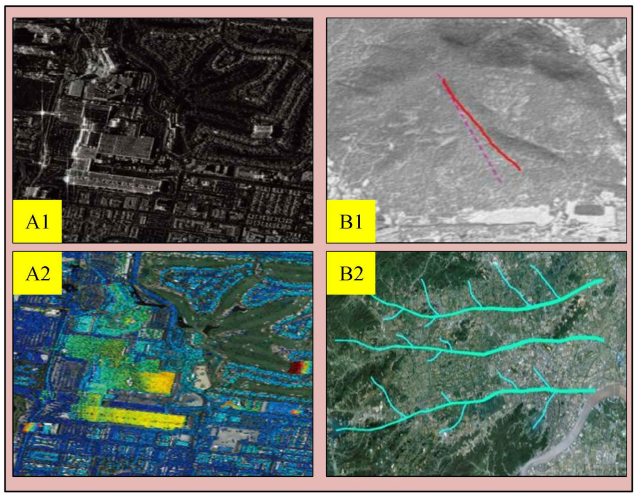

FIGURE 4. Original picture and Label picture.

and Shihmen Dam scenes. The experiment uses 500 remote sensing images of ships marked by them as data sources, including: architecture and background. We will use three different methods to classify remote sensing images. The relevant parameters of the three models are agreed to be set as: (1) Learning rate: 0.0005; (2) Number of training batches: 500; (3) Decay: 0.9995; (4) Momentum: 0.99; (5) the pre-trained model is: ResNet105, as shown in Figure 4.

III. RESULTS ANALYSIS

A. CLASSIFICATION ANALYSES OF REMOTE SENSING IMAGES

In order to verify the proposed saliency guidance and the performance of the sparse autoloader in the SAR image change detection task, the experiment in this chapter is mainly divided into two parts. The related comparison algorithm is compared with the experimental result, including the change detection result graphic and accurate of different methods. In order to verify the effectiveness of this method, five remote sensing data sets will be compared

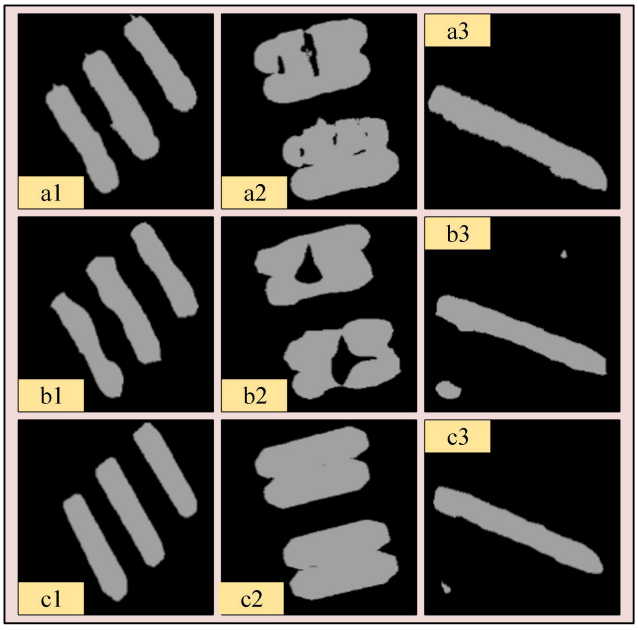

FIGURE 5. Remote sensing image classification result map.

with other excellent change detection algorithms, mainly including FCM-based Extreme Learning Machine with FCM (FCM-ELM), FCM-based Stacked Automatic Encoder wit FCM (FCM-SAE), FCM-based Supervised Contractive Auto encoders and Fuzzy Clustering (FCM-SCAE) and significant guidance based on means clustering Detection (Saliency-guided and K-means Clustering, SGK) Four change detection methods, Bern, San Francisco, Red River, and Shihmen Dam multi-temporal remote sensing images use 5 algorithms to perform the change detection experiments. The statistical values of FN, FP, OE, PCC and Kappa are reported on each data. The classification results of the remote sensing images of ships by the three models are shown in Figure 5. Figure (a) is the FC-Dense Net classification result. Figure (b) is the Deep Lab V3 model classification result, and Figure (c) is the Deep Lab V3 + classification result. It can be seen from the figure that both the FC-Dense Net model and the Deep lab V3 model have missed scoring, as showed in Figure (a2) and Figure (b2), respectively, and DeeplabV3 has a serious missing score. Deep lab V3 model and DeeplabV3 + model have the phenomenon of mis-separation, which is shown in Figure (b3) and Figure (c3) respectively. Among them, the DeeplabV3 model has serious misclassification. From a visual point of view, the Deep Lab V3 + model has the best classification effect.

The images of both resolutions are more compact, and the segmentation results are less precise, and the edges of superficial do not fit the original contours of the features, regardless of the shape or texture of the features, they will disappear as the compactness increases. You can't even see the texture state of the features at all. On the contrary, the smaller the degree of compactness, the better the edge of the segmented superficial fits the contour of the feature, and the feature information in the image can be better preserved. The size of compactness has nothing to do with the resolution of the image. The images of the two resolutions have the same change with the change of the compactness, which is the same.

It can be seen from the part marked by the red circle in the figure that when the super pixel step size S is 5, 7, or 9, the super pixels obtained in the two test areas and the original contour of the ground feature are very consistent and compact, which simplifies the image At the same time, it can retain the basic features of the features in the image to a great extent. When the super pixel step size S is 11, whether it is a high-resolution image or a low-medium resolution image, the resulting image is relatively blurry, and the original shape and texture of the feature can hardly be completely presented, or even some lines are blurred It is undesirable because it is like a ground feature. When the step size is 5, divided features are too fine, and considering that the split step size is inversely proportional to the runtime, the optimal split step size is finally selected between 7 and 9.

In order to objectively test the quality of the fused image, this section evaluates the quality of the fused image from four aspects: spectral characteristics, statistical characteristics, clarity, and information content, as showed in Table 3.

From the evaluation results of the spectral characteristics, the root mean square error (RMSE) value and the spectral distortion value (DD) of the algorithm in this paper are the smallest, indicating that the algorithm in this paper is closest to the ideal fusion image and the spectral distortion of the source image is the smallest, The highest spectral consistency with the source image. In terms of standard deviation (σ) based on statistical characteristics, the standard deviation (σ) value of the algorithm in this paper is second only to the CN algorithm, but higher than several other traditional fusion algorithms, which shows that the algorithm in this paper is relatively superior in the contrast of the fusion image. In terms of clarity, the average gradient (g) value of the fusion image of this algorithm is second only to the CN algorithm, but it is higher than several other traditional fusion algorithms. In terms of information volume, the information entropy (EN) value of the algorithm fusion image in this paper is smaller than the two algorithms CN and NND, which is higher than the other four traditional fusion methods, indicating that the image information richness after fusion is relatively good. The amount of information obtained in being relatively large. Although the algorithm in this paper is not optimal in terms of standard deviation (σ) and average gradient (g) information entropy (EN), the overall spectral characteristics and clarity are all optimal, indicating that the algorithm in this paper is relatively traditional. For the fusion algorithm, the quality of the fusion image has a great advantage.

Therefore, in terms of overall accuracy, calculation time and segmentation effect, the introduction of super pixels has greatly improved the speed of the collaborative segmentation change detection method. High-resolution images are more suitable for super-pixel-based collaborative segmentation

TABLE 3. Experiment 1 Fusion evaluation results.

Types		Spectral characteristics		Statistical characteristics	Sharpness	Amount of information
		RMSE	DD	σ	g	EN
CN-FUSE	R	22.8232	16.4177	55.1762	24.8644	7.6814
	G	22.8810	16.4999	54.7105	24.8316	7.6873
	B	23.1283	16.6929	52.5979	24.7589	7.6253
	AVG	22.9442	16.5368	54.1615	24.8183	7.6691
Brovey-FUSE	R	24.3438	18.6375	47.9969	21.7482	7.5252
	G	26.3497	20.0148	50.1939	24.1964	7.6088
	B	24.7346	18.7191	45.0998	21.9460	7.4460
	AVG	25.1427	19.1238	47.7635	22.6302	7.5430
GS-FUSE	R	23.0599	16.6678	54.7748	15.8777	7.6819
	G	24.0321	17.6002	54.3608	15.8489	7.6741
	B	24.5807	18.3475	53.2282	15.7237	7.6471
	AVG	23.8909	17.5385	54.1213	15.8168	7.6705
HSV-FUSE	R	26.1210	19.9991	54.3996	24.9884	7.6782
	G	26.1460	20.0262	53.0082	24.9130	7.6606
	B	26.1554	20.0425	50.2801	24.7299	7.5897
	AVG	26.1408	20.0226	52.5626	24.8771	7.6515
PCA-FUSE	R	22.4502	16.1390	54.1472	24.4737	7.6697
	G	22.8391	16.6114	53.9341	24.4753	7.6704
	B	23.2311	16.9284	52.2336	24.4773	7.6214
	AVG	22.8402	16.5596	53.4383	24.4754	7.6577
NND-FUSE	R	26.2907	19.9130	53.6780	25.3562	7.6692
	G	26.1528	19.8107	52.1636	25.1682	7.6430
	B	27.4021	21.3098	51.6504	24.0842	7.6328
	AVG	26.6152	20.3445	52.4974	24.8695	7.6546
PCA-FUSE	R	12.7843	9.5485	49.2723	24.9144	7.5653
	G	13.2690	10.0291	48.8111	24.9112	7.5608
	B	14.4339	11.3061	47.4004	24.8892	7.5133
	AVG	13.4957	10. 2946	48.4946	24.9049	7.5491

change detection methods, and low- and medium-resolution images are relatively unsuitable for this method. In this study, the best super pixel segmentation step for high-resolution images is 9, and for low- and medium-resolution images, you can choose according to the research needs. If you focus on the accuracy of the results, you can choose a step size of 7. If you focus on running speed, you can choose step 9. In this study, the efficiency of the experiment is emphasized, so the division step of the two experimental areas is fixed at 9.

To evaluate the classification accuracy of these three methods, we still need to start from the ACC, AA and MIOU evaluation indicators. The evaluation data come from the entire verification set. As showing in Figure 6. As can be seen from Figure 6, the classification accuracy of the FC2Dense Net ship class is 0.765, and the classification accuracy of this method is low. Classification accuracy of Deep Lab V3 ships is 0.776. DeepLabV3 + has a ship classification accuracy of 0.779, which is higher than DeepLabV3 classification accuracy, and MIOU is the highest. In comparison, DeeplabV3 + has the best classification effect.

Another key parameter in superficial segmentation is the superficial segmentation step size S. The selection of the segmentation step size greatly affects the running speed and accuracy of the subsequent collaborative segmentation change detection algorithm. If the step size is set too small, it can be maintained. Change detection accuracy, but cannot improve the speed of the algorithm, if the step size is set too large, it will increase the speed while reducing the accuracy

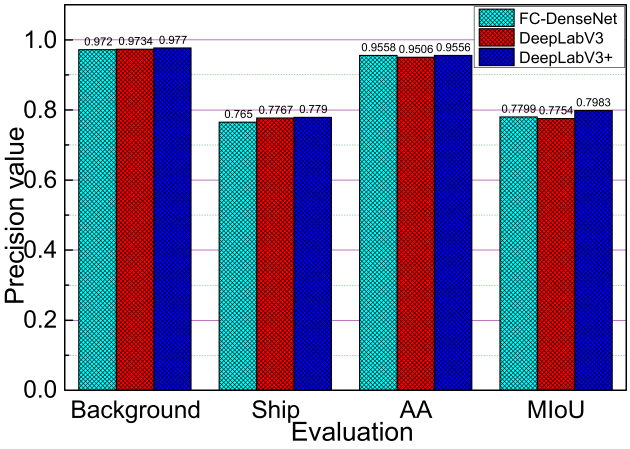

FIGURE 6. Experimental results of remote sensing images.

of the result. From the perspective of the accuracy of the detection results, the detection effect and the running time, when the superimposed analysis condition is 4, that is, the patches are merged according to the segmentation attributes of the latter phase, and the superficies of the later phase are divided into the bottom The change detection result obtained by superimposing the graphs is the best. Whether it is accurate, algorithm running time or the effect of the test results is the best of the four. The reasons for the best results of the analysis obtained by analyzing this superposition condition are as follows: Most of the changing features of the

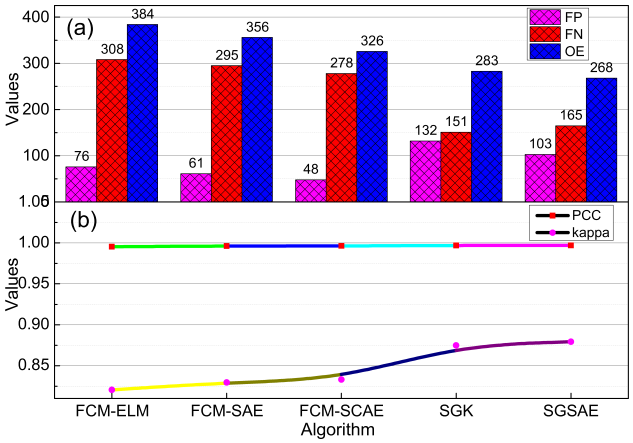

FIGURE 7. Change detection accuracy under different methods of Bern data.

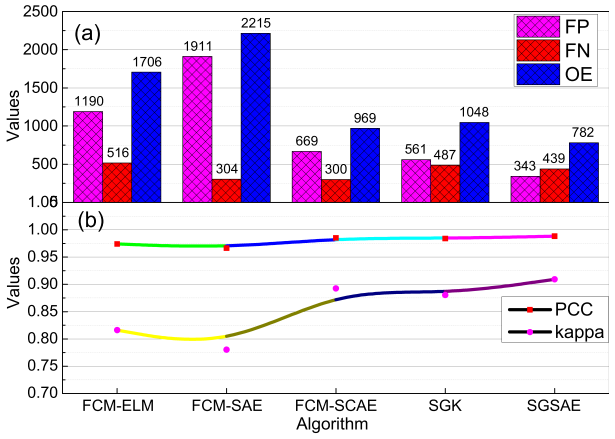

FIGURE 8. San Francisco data change detection accuracy under different methods.

two phases are increasing rather than decreasing. The contours of the changing features can be clearly detected in the image of the latter phase By the way, the changing features in the previous phase image have not yet produced an inaccurate detection of its outline and position, so the detection results of using the latter phase as the base map are more accurate.

B. DATA EXPERIMENTAL ANALYSES

In order to prove the effectiveness of the algorithm in this paper, Bern data is used for experiments. The statistical results are shown in Figure 7. In this paper, the SGSAE method obtains the best accuracy in SAR image change detection. The overall error pixels are less than other models. The OE is increased to 268, and the PCC and Kappa coefficients are better than other methods. Therefore, the SGSAE algorithm has the best performance in detecting changes in Bern data. Since the change occurs in an almost continuous area, the speckle noise in the image is not serious, and the result has been far fewer isolated pixels. Comparing the change detection result map and the ground truth map, the SGSAE method has better visual effects, which is consistent with the results in Table 3 In addition, change detection results of SGK and SGSAE have less speckle noise than the other three methods, and the visual effect is better, indicating that saliency detection helps to improve the performance of change detection.

The detection accuracy of the SGSAE method is higher than other methods, the PCC and Kappa coefficients are significantly higher than other methods, and the overall error pixels are less than other methods. Results of FCM-SCAE and SGK are slightly worse than the SGSAE method. In addition, compared with other methods, results of FCM-ELM and FCM-SAE are worse. The change detection chart is shown in Figure 8. Based on the visual results, we observe that SGSAE perform better than other methods, and it can produce better local consistency and fewer isolated pixels, and the detail retention effect is better. There are many error pixels in the change graphs of FCM-ELM and FCM-SAE, indicating that these methods have poor ability to overcome speckle noise in SAR images. The visual effects of SGK and SGSAE are better, which shows that saliency detection can reduce the effect of speckle noise. However, in the results of SGK, the existence of isolated pixels has not been well dealt with. Therefore, SGSAE has a good effect on the detection of changes in synthetic aperture radar images.

Finally, a comprehensive analysis of the results of the high scores No. 1 image and Landsat image, the running time and accuracy show that the different segmentation steps make the running speed of the two spatial resolution types of images increase to the same extent. Among them, the detection results of high-score images are good, which basically guarantees the accuracy of the changing patches, while the accuracy of Landsat image detection results is very low, and the accuracy of the patches is difficult to maintain. Therefore, when the segmentation steps of the two spatial resolution images are the same, the high-resolution images are more adaptable to super pixel segmentation, and the low- and medium-resolution images contain much feature information in one pixel before the segmentation. For high-resolution images, super pixels are used to simplify the image information on this basis, which will cause the loss of feature information and reduce the accuracy of the change detection results.

Overall, the accuracy and visual effects of TSSAE and the adaptive algorithm are not much different. Therefore, the adaptive algorithm is more suitable for this project. In order to further prove the effectiveness of the adaptive algorithm in the detection of island and reef changes, this paper uses X, Y, Z three islands and reefs for experiments, the detection accuracy is shown in Figure 9. Among them, X island reef, Y island reef, Z island reef adopts adaptive algorithm to detect the average precision of change, the accuracy rate reaches 0.9733, Kappa is 0.8090, the overall accuracy performance is better. The experiment proves that the adaptive algorithm has good performance in the change detection of high-resolution remote sensing images in the

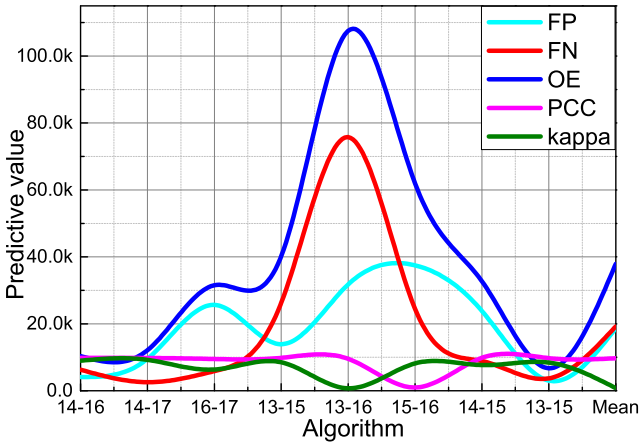

FIGURE 9. X, Y, Z islands and reefs adopt adaptive method to change detection accuracy.

island and reef area, can detect the change area very well, and has good visual effect, which meets the project requirements.

In order to verify the performance of the proposed SGSAE, Hong his data was also used in the experiment. Accuracy of the proposed SGSAE method and SGK method is significantly higher than the other three methods, OE is significantly less than other methods, PCC increased by more than 4%, and kappa increased by more than 13%. The FCM-ELM, FCM-SAE and FCM-SCAE methods have low accuracy and poor detection results. The visual effects of SGSAE and SGK methods are better. FCM-ELM, FCM-SAE and FCM-SCAE are noisier and the visual effects are poor. This is because the speckle noise in the original image is very strong, and the above method is seriously interfered by noise. The SGSAE and SGK methods both use saliency detection methods, which can well reduce the interference of coherent speckle noise. The result of SGK is worse than that of SGSAE. It can be seen that the sparse autoloader can detect the characteristics of the changing area very well, strengthen the distinction between changing pixels and non-changing pixels, and improve the detection accuracy. In addition, SGSAE has fewer false positive pixels than SGK because sparse autonomy has better classification capabilities than K-means clustering. Therefore, SGSAE can obtain better change detection results on Hong he data.

In this experiment, Shimen Dam was used to compare the detection results of the five algorithms. SGSAE has the highest accuracy of Shihmen dam data. SGSAE's kappa is improved by more than 0.04. The PCC is the highest, and the total number of false detections is the smallest. In addition, results of FCM-SAE and SGK are poor. The change detection chart of each method is shown in Figure 9. SGSAE has the best visual effect, with fewer isolated pixels and more error pixels in the other four methods. The results show that FCM-ELM, FCM-SAE and FCM-SCAE have poor ability to overcome speckle noise in SAR images, and SGK cannot effectively deal with isolated pixels, so the SGSAE detection result is the best. In summary, the proposed SGSAE has the ability to improve the detection accuracy of SAR image changes.

C. COMPARATIVE ANALYSES OF THE EXPERIMENTAL RESULTS OF THE IMPROVED ALGORITHM

In order to verify the effectiveness and practicability of the adaptive parameter estimation algorithm proposed in this paper, multiple sets of experiments with PCA, UDP, LPP, SPP, SUDP and other algorithms have been conducted on FERET, AR60, PIE, and LFW data sets. The experiment is divided into three steps: image preprocessing, running an algorithm for dimensionality reduction, and using a classifier to complete the classification task. In the process of image preprocessing, the pictures in each data set are cropped to the corresponding size, and then processed into a gray scale image, and finally the pixels in the picture are processed into a vector by row, and the vectors are sequentially arranged into a data matrix. In the process of dimensionality reduction, the data set is first divided into a training set and a test set, then the algorithm is run on the training set to obtain a projection matrix, and finally the test set is also reduced to the same dimension through the obtained projection matrix. For UDP and LPP algorithms, first find the most suitable number of neighbors, and then reduce the training set to different dimensions; for PCA, SPP and the algorithm proposed in this chapter, directly reduce the dimension, and also reduce the training set to different dimensions. In the classification task, all algorithms finally use the nearest neighbor classifier to complete the classification task and obtain the corresponding classification accuracy. The experimental results are shown in Figure 10.

The experimental results on the four data sets of FERET, AR60, PIE, and LFW show that the adaptive parameter estimation algorithm proposed in this paper has the best effect on the three experimental sets, especially on the AR60 data set, which is better The recognition rate increased by 12 percentage points. In addition, the recognition rate on the PIE dataset is also less than 1 percentage point compared to the highest LPP algorithm. Experimental results prove the effectiveness of the algorithm. The other five algorithms compared with the adaptive parameter estimation algorithm proposed in this paper are all unsupervised algorithms. These algorithms do not use the category information of the samples. Therefore, in the classification task, the performance of these five algorithms is worse than that of adaptive parameter estimation. The adaptive parameter estimation algorithm is a supervised extension of SUDP. The advantages of SUDP such as sparsity and locality are also inherited in the adaptive parameter estimation algorithm. In addition, since the adaptive parameter estimation is to sparsely represent the samples of the same kind, in the process of solving the sparse representation, the number of participating samples is small, which improves the efficiency of the sparse reconstruction of the adaptive parameter estimation algorithm. Although no specific experiments have been done to prove it, from the

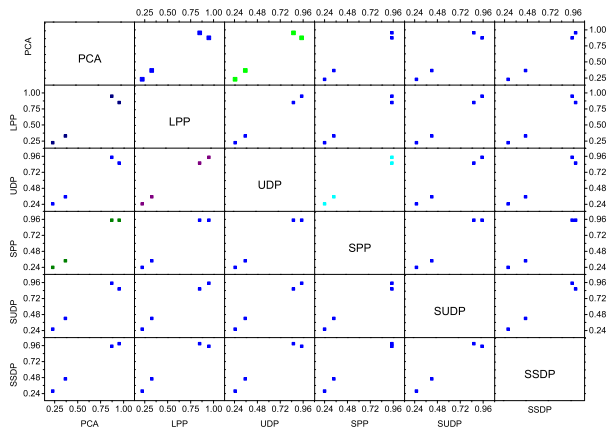

FIGURE 10. The recognition rate of each algorithm on each data set.

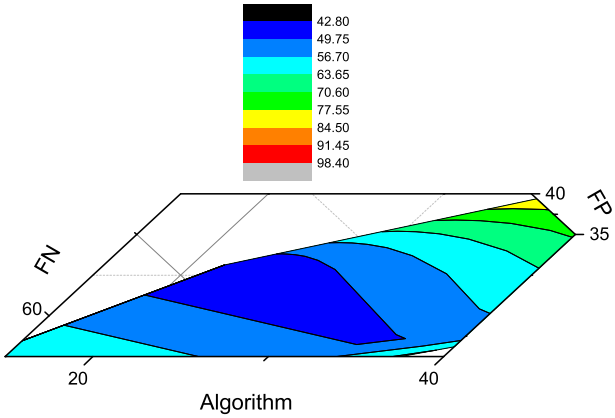

FIGURE 11. Comparison of adaptive parameter estimation and SUDP.

intuitive experience during the experiment, the running speed of the adaptive parameter estimation is higher.

In order to comprehensively measure the experimental results and increase the reliability of the experimental results, the five methods of FCM-ELM, FCM-SAE and FCM-SCAE, SGK and SGSAE were used to count the FN, FP, OE, PCC and Kappa of 4 SAR image data. It can be seen from Figure 10 that SGSAE have the smallest false detection rate, the best accuracy and Kappa coefficient performance, and has excellent SAR remote sensing image change detection performance. It has been verified that the salient region detection in this method can extract potential change regions and remove background pixels, which can weaken the effect of speckle. The HFCM model can select more reliable samples as the training set, making the proposed method an unsupervised method. In addition, the sparse autoloader has the ability to obtain the features of two original SAR images and the difference image. Experiments show that performance of the proposed SGSAE is better than other related change detection methods.

It can be seen from Figure 11 that the recognition rate of the adaptive parameter estimation algorithm on FERET, ORL, AR60, Yale and other four data sets is higher than that of SUDP, especially on the AR60 data set, the adaptive parameter estimation algorithm is better than adaptive The effect of the parameter estimation algorithm is 10 percentage points higher. Although the recognition rate of the adaptive parameter estimates is lower than that of SUDP on the AR and PIE data sets, it does not exceed 2 percentage points. These experimental results can prove that the recognition rate of the adaptive parameter estimation is improved compared with SUDP.

From the perspective of the accuracy of the detection results, the detection effect and the running time, when the superimposed analysis condition is 4, that is, the patches are merged according to the segmentation attributes of the latter phase, and the super pixels of the later phase are divided into the bottom The change detection result obtained by superimposing the graphs is the best. Whether it is accurate, algorithm running time or the effect of the test results is the best of the four. The reasons for the best results of the analysis obtained by analyzing this superposition condition are as follows: Most of the changing features in the two phases are increasing rather than decreasing. The contours of the changing features can be clearly detected in the image of the latter phase By the way, the changing features in the previous phase image have not yet produced an inaccurate detection of its contour and position, so the detection results using the latter phase as the base map are more accurate.

The overall recognition rate of adaptive parameter estimation has been improved because of adding the category information of the sample. The advantage of this is that it can more accurately reflect the geometric relationship between the sample points during sparse reconstruction. Note that on the AR60 dataset, the recognition rate of the adaptive parameter estimation has been greatly improved compared to SUDP.

It can be speculated that the influence of pseudo-neighbor points on this data set may be relatively large. The pseudo-neighbor point has a greater impact on the SUDP algorithm, which makes the SUDP algorithm interfere with sparse reconstruction, and assigns a larger weight to the non-homogeneous neighbor points, resulting in the reconstruction of the sparse matrix cannot be well reflected The geometric relationship between samples. However, in adaptive parameter estimation, sparse reconstruction only occurs between similar samples, limiting the effect of pseudo-nearest neighbors, and in the process of solving the objective function, there are minimum and maximum constraints within the class, these Factors have led to this result. Note that the accuracy of the adaptive parameter estimation algorithm on the PIE data set is not much improved compared to the SUDP algorithm. The reason may be that the PIE data set has obvious characteristics. On this data set, both algorithms can complete the dimensionality reduction task well, and get a good recognition rate through the classifier. Therefore, the label information used in the adaptive parameter estimation algorithm. And global constraints do not bring great advantages to the PIE data set.

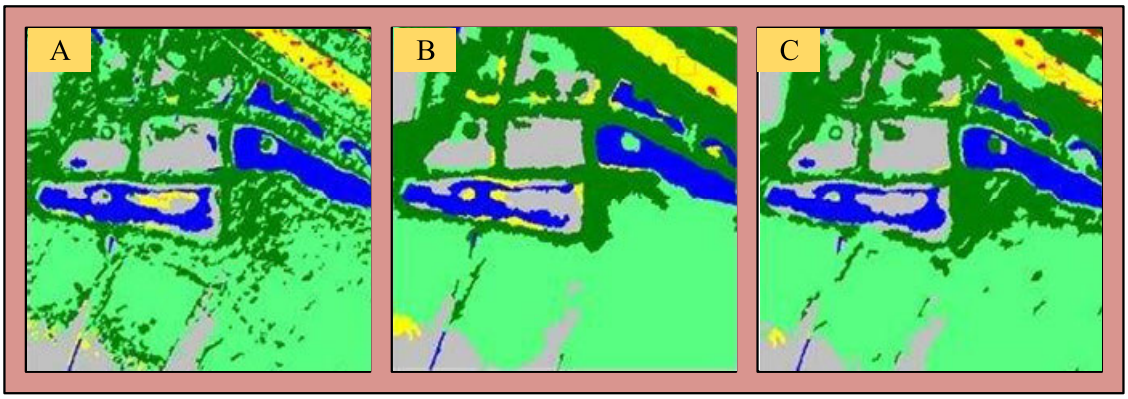

FIGURE 12. Classification graphs of remote sensing graphics with different algorithms.

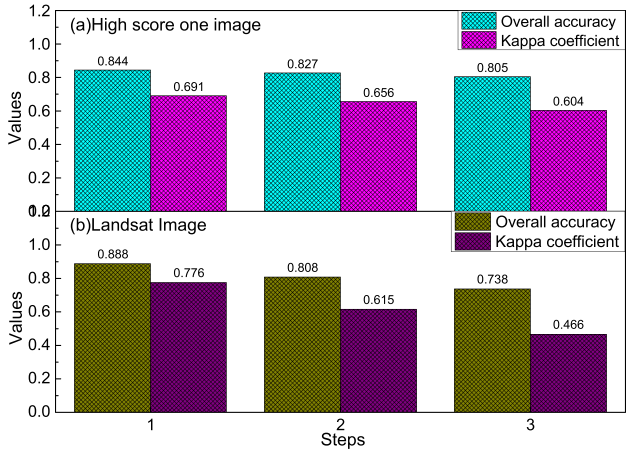

FIGURE 13. Comparison of adaptive parameter estimation and SUDP.

As showed in Figure 12, it is the classification map of remote sensing graphics of different algorithms. Figure 12 (A), Figure 12 (B), and Figure 12 (C) are the classification results of FC-Dense Net model, DeeplabV3 model, and Deep Lab V3 + model. In FC-Dense Net classification results, in Figure 12 (A), there is a phenomenon that the background is mistakenly classified as vegetation or vegetation. In the classification results of Deep Lab V3, the roads in Figure 12 (B) are coherent. In the classification results of DeeplabV3 +, a small part of the road in Figure 12(C) was mistakenly classified as background.

In order to verify the accuracy of the segmentation results, this paper uses a confusion matrix to check the accuracy in e Cognition software. This paper selects a certain amount of changing and non-changing samples in the experimental area, and evaluates the accuracy of the test results by calculating the error matrix and Kappa coefficient. Figure 13 is a comparison of the overall accuracy, Kappa coefficient, and running time of the six change detection results.

The calculation time is closely related to the superficial step size, and the shortest can reach no more than 4 hours. The change detection running time of the two different spatial resolution images is reduced with the increase of the step size, and the degree of reduction is almost the same, from more than one day to about 3.5 hours. It can be seen that the size of the superficial segmentation step is the running time has nothing to do with the spatial resolution of the image. Secondly, the accuracy of the results of the two resolution images decreases with the increase of the superficial step size. Accuracy of the GAO fen was reduced from 0.844 to 0.805, while the accuracy of the Landsat image was reduced from 0.888 to 0.738. The detection accuracy of the changes in both resolutions is reduced to varying degrees, and it is inevitable to analyze this situation theoretically. Because the definition of superficial is to simplify the information in the image to improve the efficiency of image processing, the accuracy of the results using superficial segmentation should be lower than the accuracy of non-super pixel segmentation. However, the accuracy of high-resolution images is lower than that of low- and medium-resolution images. The overall accuracy of high-resolution images is reduced by 0.04, while that of low- and medium-resolution images is reduced by 0.15. Therefore, the size of the superficial segmentation step has a great relationship with the spatial resolution of the image in terms of the accuracy of the result.

IV. CONCLUSION

This paper proposes a SAR remote sensing image change detection algorithm based on an autoloader with adaptive parameter estimation. Generally speaking, the change is in the initial differential image has good local consistency and global prominence. In order to mitigate the influence of coherent speckle noise on the detection results, the significant change area can be detected by using significant area detection and thresholds to extract changes Area, exclude the interference of noise outside the area. Hierarchical FCM clustering is used to automatically generate training samples to improve the reliability of the samples. In order to increase the distinction between the change area and the non-change area, and better extract the change information, the deep neural network of the sparse autoloader is used to

generate a more complete and detailed change detection map to improve the accuracy of change detection. Experimental results show that the algorithm has good ability to suppress coherent speckle noise, and can well the noise removal and retain the details of changes, extract the change are more finely and accurately, and is more suitable for SAR image change detection. Histogram matching method is used for color balance to eliminate the influence of color difference of images in different time phases. Then, for environmental interference factors such as weather, the target segmentation algorithm can be used to extract the target area and exclude the influence of the background. Then, use principal component analysis and k-means clustering to process the difference map, reduce the isolated pixels, and obtain the change area. Finally, after the noise filtering, the final difference map is obtained. Experiments were carried out using 4 sets of image data of islands and reefs. The experimental results show that the detection accuracy of the algorithm is high, which can effectively reduce the interference of the external environment on change detection, especially for the interference outside the target area such as seawater fluctuations and ships. It can well extract the change area of the island and reef area. The research in this article will have a huge impact on the future.

REFERENCES

[1] R. Touati, M. Mignotte, and M. Dahmane, "A reliable mixed-norm-based multiresolution change detector in heterogeneous remote sensing images," *IEEE J. Sel. Topics Appl. Earth Observ. Remote Sens.*, vol. 12, no. 9, pp. 3588–3601, Sep. 2019.

[2] G. Cao, X. Li, and L. Zhou, "Unsupervised change detection in high spatial resolution remote sensing images based on a conditional random field model," *Eur. J. Remote Sens.*, vol. 49, no. 1, pp. 225–237, Jan. 2016.

[3] F. Hu, J. Wu, L. Chang, and R. F. Hanssen, "Incorporating temporary coherent scatterers in multi-temporal InSAR using adaptive temporal subsets," *IEEE Trans. Geosci. Remote Sens.*, vol. 57, no. 10, pp. 7658–7670, Oct. 2019.

[4] W.-K. Baek and H.-S. Jung, "A review of change detection techniques using multi-temporal synthetic aperture radar images," *Korean J. Remote Sens.*, vol. 35, no. 5, pp. 737–750, 2019.

[5] E. A. Storey, D. A. Stow, L. L. Coulter, and C. Chen, "Detecting shadows in multi-temporal aerial imagery to support near-real-time change detection," *GIScience Remote Sens.*, vol. 54, no. 4, pp. 453–470, Jul. 2017.

[6] M. Farahani and A. Mohammadzadeh, "Domain adaptation for unsupervised change detection of multisensor multitemporal remote-sensing images," *Int. J. Remote Sens.*, vol. 41, no. 10, pp. 3902–3923, May 2020.

[7] L. Cai, W. Shi, H. Zhang, and M. Hao, "Object-oriented change detection method based on adaptive multi-method combination for remote-sensing images," *Int. J. Remote Sens.*, vol. 37, no. 22, pp. 5457–5471, Nov. 2016.

[8] M. Han, C. Zhang, and Y. Zhou, "Object-wise joint-classification change detection for remote sensing images based on entropy query-by fuzzy ARTMAP," *GISci. Remote Sens.*, vol. 55, no. 2, pp. 265–284, Mar. 2018.

[9] A. Asokan and J. Anitha, "Change detection techniques for remote sensing applications: A survey," *Earth Sci. Informat.*, vol. 12, no. 2, pp. 143–160, Jun. 2019.

[10] Z. Liu, G. Li, G. Mercier, Y. He, and Q. Pan, "Change detection in heterogenous remote sensing images via homogeneous pixel transformation," *IEEE Trans. Image Process.*, vol. 27, no. 4, pp. 1822–1834, Apr. 2018.

[11] C. Luo and S. Cui, "SAR image change detection based on Monte Carlo sampling," *Remote Sens. Lett.*, vol. 9, no. 11, pp. 1050–1059, Nov. 2018.

[12] Z. Li, W. Shi, M. Hao, and H. Zhang, "Unsupervised change detection using spectral features and a texture difference measure for VHR remote-sensing images," *Int. J. Remote Sens.*, vol. 38, no. 23, pp. 7302–7315, Dec. 2017.

[13] M. A. Clement, C. G. Kilsby, and P. Moore, "Multi-temporal synthetic aperture radar flood mapping using change detection," *J. Flood Risk Manage.*, vol. 11, no. 2, pp. 152–168, Jun. 2018.

[14] A. Safari, H. Sohrabi, S. Powell, and S. Shataee, "A comparative assessment of multi-temporal landsat 8 and machine learning algorithms for estimating aboveground carbon stock in coppice oak forests," *Int. J. Remote Sens.*, vol. 38, no. 22, pp. 6407–6432, Nov. 2017.

[15] P. Chen, Z. Jia, J. Yang, and N. Kasabov, "Unsupervised change detection of SAR images based on an improved NSST algorithm," *J. Indian Soc. Remote Sens.*, vol. 46, no. 5, pp. 801–808, May 2018.

[16] A. Ben Abbes, O. Bounouh, I. R. Farah, R. de Jong, and B. Martínez, "Comparative study of three satellite image time-series decomposition methods for vegetation change detection," *Eur. J. Remote Sens.*, vol. 51, no. 1, pp. 607–615, Jan. 2018.

[17] A. M. Lal and S. M. Anouncia, "Enhanced dictionary based sparse representation fusion for multi-temporal remote sensing images," *Eur. J. Remote Sens.*, vol. 49, no. 1, pp. 317–336, Jan. 2016.

[18] S. Liu, D. Marinelli, L. Bruzzone, and F. Bovolo, "A review of change detection in multitemporal hyperspectral images: Current techniques, applications, and challenges," *IEEE Geosci. Remote Sens. Mag.*, vol. 7, no. 2, pp. 140–158, Jun. 2019.

[19] W. Ma, Y. Wu, M. Gong, Y. Xiong, H. Yang, and T. Hu, "Change detection in SAR images based on matrix factorisation and a bayes classifier," *Int. J. Remote Sens.*, vol. 40, no. 3, pp. 1066–1091, Feb. 2019.

[20] W. Liu, R. Qin, and F. Su, "Weakly supervised classification of time-series of very high resolution remote sensing images by transfer learning," *Remote Sens. Lett.*, vol. 10, no. 7, pp. 689–698, Jul. 2019.

[21] R. Al-Ruzouq, K. Hamad, A. Shanableh, and M. Khalil, "Infrastructure growth assessment of urban areas based on multi-temporal satellite images and linear features," *Ann. GIS*, vol. 23, no. 3, pp. 183–201, Jul. 2017.

[22] S. Xie, L. Liu, X. Zhang, and X. Chen, "Annual land-cover mapping based on multi-temporal cloud-contaminated landsat images," *Int. J. Remote Sens.*, vol. 40, no. 10, pp. 3855–3877, May 2019.

[23] L. Wan, Y. Xiang, and H. You, "A post-classification comparison method for SAR and optical images change detection," *IEEE Geosci. Remote Sens. Lett.*, vol. 16, no. 7, pp. 1026–1030, Jul. 2019.

[24] X. Zhang, R. Fan, L. Ma, X. Liao, and X. Chen, "Change detection in very high-resolution images based on ensemble CNNs," *Int. J. Remote Sens.*, vol. 41, no. 12, pp. 4757–4779, Jun. 2020.

[25] S. Pathan and P. Thakre, "Fuzzy clustering technique and PCA based unsupervised change detection method in multitemporal SAR images," *Int. J. Eng. Manage. Res. (IJEMR)*, vol. 7, no. 1, pp. 345–348, 2017.

[26] M. Hasanlou, S. T. Seydi, and R. Shah-Hosseini, "A sub-pixel multiple change detection approach for hyperspectral imagery," *Can. J. Remote Sens.*, vol. 44, no. 6, pp. 601–615, Nov. 2018.

[27] H. Ben-Romdhane, M. Al-Musallami, P. R. Marpu, T. B. M. J. Ouarda, and H. Ghedira, "Change detection using remote sensing in a reef environment of the UAE during the extreme event of el Niño 2015–2016," *Int. J. Remote Sens.*, vol. 39, no. 19, pp. 6358–6382, Oct. 2018.

[28] H. Zhuang, K. Deng, H. Fan, and S. Ma, "A novel approach based on structural information for change detection in SAR images," *Int. J. Remote Sens.*, vol. 39, no. 8, pp. 2341–2365, Apr. 2018.

[29] M. Janalipour and M. Taleai, "Building change detection after earthquake using multi-criteria decision analysis based on extracted information from high spatial resolution satellite images," *Int. J. Remote Sens.*, vol. 38, no. 1, pp. 82–99, Jan. 2017.

[30] C. P. Dalmiya, N. Santhi, and B. Sathyabama, "A novel feature descriptor for automatic change detection in remote sensing images," *Egyptian J. Remote Sens. Space Sci.*, vol. 22, no. 2, pp. 183–192, Aug. 2019.

[31] W. Xiao, S. Xu, S. O. Elberink, and G. Vosselman, "Individual tree crown modeling and change detection from airborne lidar data," *IEEE J. Sel. Topics Appl. Earth Observ. Remote Sens.*, vol. 9, no. 8, pp. 3467–3477, Aug. 2016.

[32] M. Hasanlou and S. T. Seydi, "Automatic change detection in remotely sensed hyperspectral imagery (case study: Wetlands and waterbodies)," *Earth Observ. Geomatics Eng.*, vol. 2, no. 1, pp. 9–25, Jun. 2018.

[33] M. Yang, L. Jiao, F. Liu, B. Hou, and S. Yang, "Transferred deep learning-based change detection in remote sensing images," *IEEE Trans. Geosci. Remote Sens.*, vol. 57, no. 9, pp. 6960–6973, Sep. 2019.

[34] S. Liu, Y. Zheng, M. Dalponte, and X. Tong, "A novel fire index-based burned area change detection approach using Landsat-8 OLI data," *Eur. J. Remote Sens.*, vol. 53, no. 1, pp. 104–112, Jan. 2020.

[35] K. K. Thyagharajan and T. Vignesh, "Soft computing techniques for land use and land cover monitoring with multispectral remote sensing images: A review," *Arch. Comput. Methods Eng.*, vol. 26, no. 2, pp. 275–301, Apr. 2019.
[36] S. Ji, Z. Zhang, C. Zhang, S. Wei, M. Lu, and Y. Duan, "Learning discriminative spatiotemporal features for precise crop classification from multi-temporal satellite images," *Int. J. Remote Sens.*, vol. 41, no. 8, pp. 3162–3174, Apr. 2020.
[37] M. Pirnazar, K. Ostad-Ali-Askari, and S. Eslamian, "Change detection of urban land use and urban expansion using GIS and RS, case study: Zanjan province, Iran," *Int. J. Constructive Res. Civil Eng.*, vol. 4, no. 10, pp. 2454–8693, 2018.
[38] D. C. Wickramasinghe, T. T. Vu, and T. Maul, "Satellite remote-sensing monitoring of a railway construction project," *Int. J. Remote Sens.*, vol. 39, no. 6, pp. 1754–1769, Mar. 2018.
[39] D. Li, F. Yang, and X. Wang, "Study on ensemble crop information extraction of remote sensing images based on SVM and BPNN," *J. Indian Soc. Remote Sens.*, vol. 45, no. 2, pp. 229–237, Apr. 2017.
[40] D. Marinelli, F. Bovolo, and L. Bruzzone, "A novel change detection method for multitemporal hyperspectral images based on binary hyperspectral change vectors," *IEEE Trans. Geosci. Remote Sens.*, vol. 57, no. 7, pp. 4913–4928, Jul. 2019.
[41] L. Zhou, G. Cao, Y. Li, and Y. Shang, "Change detection based on conditional random field with region connection constraints in high-resolution remote sensing images," *IEEE J. Sel. Topics Appl. Earth Observ. Remote Sens.*, vol. 9, no. 8, pp. 3478–3488, Aug. 2016.
[42] H. Zhuang, H. Fan, K. Deng, and Y. Yu, "An improved neighborhood-based ratio approach for change detection in SAR images," *Eur. J. Remote Sens.*, vol. 51, no. 1, pp. 723–738, Jan. 2018.
[43] W. Cao, A. Twele, S. Plank, and S. Martinis, "A three-class change detection methodology for SAR-data based on hypothesis testing and Markov Random field modelling," *Int. J. remote Sens.*, vol. 39, no. 2, pp. 488–504, Jan. 2018.
[44] R. C. Percy, "Segmentation of remotely sensed images using unsupervised 'Sampling-Resampling' based on hopfield type neural network," *Int. J. Eng. Comput. Sci.*, vol. 7, no. 2, pp. 23606–23612, 2018.
[45] C. R. Hakkenberg, M. P. Dannenberg, C. Song, and K. B. Ensor, "Characterizing multi-decadal, annual land cover change dynamics in houston, TX based on automated classification of landsat imagery," *Int. J. Remote Sens.*, vol. 40, no. 2, pp. 693–718, Jan. 2019.
[46] P. Liu, P. J. Du, and R. M. Han, "Modeling spatial and temporal change of soil erosion based on multi-temporal remotely sensed data," *Sci. Cold Arid Regions*, vol. 7, no. 6, pp. 702–708, Nov. 2018.
[47] O. Einav, D. Geva, D. Yoeli, M. Kerzhner, and K.-H. Mauritz, "Development and validation of the first robotic scale for the clinical assessment of upper extremity motor impairments in stroke patients," *Topics Stroke Rehabil.*, vol. 18, no. 1, pp. 587–598, Oct. 2011.
[48] H. Zhiqiang, Z. Ning, and S. U. Zhaoyuan, "Effects of pricking and cupping combined with rehabilitation training on elbow flexion spasticity of upper limb after stroke and its IEMG value," *Chin. Acupuncture Moxibustion*, vol. 38, no. 2, pp. 119–125, Feb. 2018.
[49] P. Standen, K. Threapleton, A. Richardson, L. Connell, D. Brown, S. Battersby, F. Platts, and A. Burton, "A low cost virtual reality system for home based rehabilitation of the arm following stroke: A randomised controlled feasibility trial," *Clin. Rehabil.*, vol. 31, no. 3, pp. 340–350, Mar. 2017.
[50] T. Fujita, A. Sato, Y. Yamamoto, K. Otsuki, K. Tsuchiya, and F. Tozato, "Motor function cutoff values for independent dressing in stroke patients," *Amer. J. Occupational Therapy*, vol. 70, no. 3, Apr. 2016, Art. no. 7003290010p1.

YU CHEN was born in Hubei, China, in 1976. He was received the bachelor's degree from Northeastern University, Shenyang, Liaoning, in 2001, and the M.E. and Ph.D. degrees from the China University of Geosciences, Wuhan, Hubei, China, in 2004 and 2007, respectively. Since 2007, he has been a Lecturer with the School of Geography and Information Engineering, China University of Geosciences. He was a Visiting Scholar with the Department of Geoscience and Remote Sensing, Delft University of Technology, The Netherlands, from 2017 to 2018. His current research interests are the remote sensing data processing and information extraction, and remote sensing geological disaster monitoring application combined with GNSS, theory and application of GPS meteorological precipitable water vapor inversion calculation, and GPS modeling and positioning calculation.

ZUTAO MING was born in Jiayu, Hubei, China, in 1969. He received the bachelor's degree from the Wuhan University of Surveying and Mapping, in 1994. He was an Associate Professor with the School of Geography and Information Engineering, China University of Geosciences, Wuhan, China, in 2004. His interests are remote sensing geological disaster prediction model building and calculation in high-speed railway's bridge and tunnel, and engineering deformation monitoring surveying, and measurement adjustment and program calculation.

MASSIMO MENENTI was born in Italy, in 1949. He received the degree in physics from the University of Rome and the Ph.D. degree in environmental sciences from the University of Wageningen. He is a Full Professor in optical and laser remote sensing with the Department of Geoscience and Remote Sensing, Faculty of Civil Engineering, Delft University of Technology, The Netherlands. His research interests are land surface processes and remote sensing with emphasis on hydrology and water management. In recent years, he has coordinated the EU research project hydrological determinants of agricultural production in South America. He is currently the Coordinator of an EU network dealing with Climate Impact on Water and Dry lands Agriculture (CLIWARDA). He has coordinated a series of scientific studies towards the development of the Surface Processes and Ecosystem Changes Through Response Analysis (SPECTRA) Mission for the European Space Agency. He is also currently a Coordinator of the FP7 Environment Project "A Prototype Observation System for Water Resources in South–East Asia: Ground and Space Measurements to Support Hydrological and Atmospheric Modeling of the Qinghai–Tibet Plateau (CEOP – AEGIS)" carried out by 17 organizations in eight countries.